
**Aerosol Science and Technology**
Publication details, including instructions for authors and subscription information:
http://www.informaworld.com/smpp/title~content=t713656376

# Interpretation of Secondary Organic Aerosol Formation from Diesel Exhaust Photooxidation in an Environmental Chamber

Shunsuke Nakao[ab]; Manish Shrivastava[bcd]; Anh Nguyen[bc]; Heejung Jung[bc]; David Cocker III[ab]
[a] Department of Chemical and Environmental Engineering, University of California, Riverside, California, USA [b] College of Engineering, Center for Environmental Research and Technology (CE-CERT), University of California, Riverside, California, USA [c] Department of Mechanical Engineering, University of California, Riverside, California, USA [d] Pacific Northwest National Laboratory, Richland, Washington, USA

Accepted uncorrected manuscript posted online: 23 March 2011

First published on: 14 April 2011

**To cite this Article** Nakao, Shunsuke , Shrivastava, Manish , Nguyen, Anh , Jung, Heejung and Cocker III, David(2011) 'Interpretation of Secondary Organic Aerosol Formation from Diesel Exhaust Photooxidation in an Environmental Chamber', Aerosol Science and Technology, 45: 8, 954 — 962, First published on: 14 April 2011 (iFirst)
**To link to this Article: DOI:** 10.1080/02786826.2011.573510
**URL:** http://dx.doi.org/10.1080/02786826.2011.573510

*Aerosol Science and Technology*, 45:954–962, 2011

ISSN: 0278-6826 print / 1521-7388 online
DOI: 10.1080/02786826.2011.573510

# Interpretation of Secondary Organic Aerosol Formation from Diesel Exhaust Photooxidation in an Environmental Chamber

**Shunsuke Nakao,[1,2] Manish Shrivastava,[2,3,4] Anh Nguyen,[2,3] Heejung Jung,[2,3] and David Cocker III[1,2]**

[1]*Department of Chemical and Environmental Engineering, University of California, Riverside, California, USA*
[2]*College of Engineering, Center for Environmental Research and Technology (CE-CERT), University of California, Riverside, California, USA*
[3]*Department of Mechanical Engineering, University of California, Riverside, California, USA*
[4]*Pacific Northwest National Laboratory, Richland, Washington, USA*



**Secondary organic aerosol (SOA) formation from diesel exhaust was investigated using an environmental chamber. Particle volume measurement based solely on mobility diameter underestimated the SOA formation from diesel exhaust due to the external void space of agglomerate particles. Therefore, particle mass concentration and fractal-like dimension was determined from the particle effective density as a function of particle mass using an aerosol particle mass analyzer and scanning mobility particle sizer (APM–SMPS). Continuous aging of aerosol measured by an increase of atomic ratio (O/C) underscored the importance of multigenerational oxidation of low-volatile organic vapors emitted from diesel engine as a possible significant source of ambient oxygenated SOA. Higher particle effective densities were observed when raw exhaust was injected into a full bag as opposed to filling a bag with diluted exhaust using an ejector diluter. This suggests that the dilution method, in addition to dilution ratio, may impact the evaporation of semivolatile species. This study demonstrates the critical need to evaluate particle mass when evaluating SOA formation onto fractal particles such as diesel exhaust.**

Received 12 November 2010; accepted 10 March 2011.

This material is based in part upon work supported by the National Science Foundation under grant number ATM-0449778. Any opinions, findings, and conclusions or recommendations expressed in this material are those of the authors and do not necessarily reflect the views of the National Science Foundation. We also gratefully acknowledge funding support from the W. M. Keck Foundation, University of California Transportation Center (UCTC), and Department of Chemical and Environmental Engineering, University of California, Riverside. We also thank Dr. Quentin Malloy for initial experimental setup and Dr. Li Qi and Ms. Ping Tang for helping in data processing. Ms. Nguyen acknowledges support from NSF GRF (ATM-2010096512) and UCTC.

Address correspondence to David Cocker, Center for Environmental Research and Technology, 1084 Columbia Avenue, Riverside, CA 92507, USA. E-mail: dcocker@engr.ucr.edu

## 1. INTRODUCTION

Organic aerosol (OA) accounts for ∼20%–90% of aerosol mass in the lower troposphere (Kanakidou et al. 2005). OA contributes to global climate change (Kanakidou et al. 2005; IPCC 2007), adverse human health risks (Davidson et al. 2005; Pope and Dockery 2006), and visibility reduction (Eldering and Cass 1996). Air quality models using parameters developed from environmental chamber studies severely underpredict OA in the atmosphere pointing towards large uncertainties including "missing precursors" and physicochemical processes governing formation and evolution of OA in the atmosphere (Volkamer et al. 2006).

OA is classified into two categories: (1) primary OA (POA) that is directly emitted from sources as particles and (2) secondary OA (SOA) that is formed in the atmosphere from photochemical oxidation of organic vapors followed by gas to particle partitioning. Additionally, semivolatile components of POA evaporate to release semivolatile organic compounds (SVOCs) and intermediate volatility organic compounds (IVOCs), which easily form SOA in the atmosphere due to their lower volatility (Shrivastava et al. 2006; Robinson et al. 2007; Chan et al. 2009; Donahue et al. 2009; Grieshop et al. 2009; Presto et al. 2009). Diesel exhaust is a major source of urban POA (Schauer et al. 1996). Additionally, Robinson et al. (2007) observed rapid and high SOA formation from photooxidation of diesel exhaust in an environmental chamber. However, recent studies by Samy and Zielinska (2010) and Chirico et al. (2010) observed insignificant SOA formation from diesel exhaust without the addition of radical sources or additional hydrocarbons. As a result, further investigation is required to identify causes of this discrepancy.

The mass of SOA formed from diesel exhaust is often calculated on the basis of the increase of wall-loss-corrected

particle volume concentration multiplied by a unit density (1.0 g/cm$^3$) with the assumption of spherical particles (Robinson et al. 2007; Weitkamp et al. 2007; Chirico et al. 2010; Samy and Zielinska 2010). However, this assumption is often not valid for diesel agglomerate particles. Park et al. (2003) and Maricq et al. (2000) reported that effective density decreases as particle size increases because of increasing void space due to agglomeration. Weitkamp et al. (2007) observed that coating SOA onto a fractal-like diesel particle increases particle density.

This study investigated the changes in effective density of diesel agglomerates during partitioning of secondary organic species onto particles. Also, the impact of different dilution methodologies on the diesel particles' effective density evolution in an environmental chamber was investigated for the first time. Furthermore, chemical evolution (aging) of diesel exhaust was examined to evaluate the importance of multigenerational photochemical oxidation of diesel exhaust leading to SOA formation.

## 2. EXPERIMENTAL

All experiments were conducted in the mezzanine chamber located at the Center for Environmental Research and Technology, College of Engineering, University of California, Riverside (CE-CERT/UC). A schematic diagram is shown in Figure 1. The chamber is in a 2.5 m × 3 m × 7.8 m enclosure covered with reflective aluminum sheets and is illuminated with 170 of 40 W black lights with peak intensity at 350 nm (350 BL, SYLVANIA) with the $NO_2$ photolysis rate of 0.6 min$^{-1}$. Within this enclosure is a 12 m$^3$ volume 2-mil (50.8 $\mu$m) FEP Teflon chamber. A minimum of 1-m space between the chamber surface and black lights was maintained to avoid excessive heating at the surface of the film. Additionally, six fans are used to mix the air inside the enclosure with conditioned room air to minimize heating within the enclosure. The enclosure temperature is typically within 25°C–28°C. Prior to every experiment, the chamber is flushed overnight with pure air [Aadco 737 series air purification system]. Background particle concentration is below the detection limit of 0.2 cm$^{-3}$.

Dilution of diesel exhaust was performed in two ways: (1) "ejector dilution" in which a custom built two-stage ejector dilution system as described by Khalek et al. (2000) was used and (2) "in-chamber dilution" in which raw exhaust was injected into the chamber already filled with clean air. The ejector dilution involves intensive mixing of raw exhaust and compressed clean filtered air. On the other hand, during the "in-chamber dilution," dilution occurs only by slow mixing of the raw exhaust and the clean air inside the chamber. The ejector dilution is followed by transfer in either a short (2 m) or long transfer line (16 m, ~5 cm I.D., copper) (Figure 1a and c). The in-chamber dilution occurs after transfer of undiluted exhaust in a short transfer line (Figure 1b).

Diesel exhaust was obtained from a Pramac 3.6 kW generator (E3750 MYHDI, Yanmar Engine). This is the similar type of engine as used by Robinson et al. (2007). The engine was

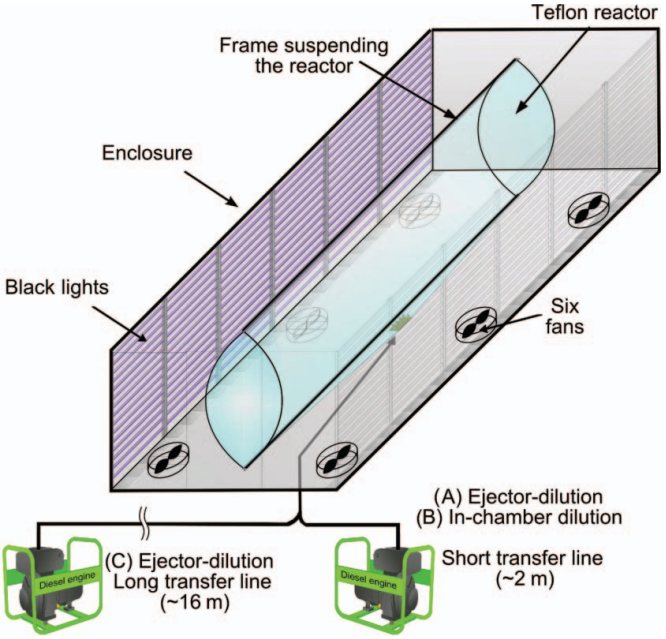


FIG. 1. A schematic diagram of the College of Engineering-Center for Environmental Research and Technology, University of California, Riverside (CE-CERT/UC) mezzanine chamber.

connected to a resistive load bank (Swift-E STD, Simplex, Inc.). The engine was operated on ultra low sulfur diesel (ULSD) fuel (<15 ppmS) at 50% (medium) load, 30% (low) load, and for idling condition. The engine was warmed-up for 45 min prior to injection to allow the diesel exhaust to reach steady state.

Particle size distribution between 27 and 685 nm was monitored by a scanning mobility particle sizer (SMPS) similar to that described by Cocker et al. (2001). Particle sizing was periodically verified by aerosolized polystyrene latex (PSL) particles (90, 220, and 350 nm) (3000 series Nanosphere Size Standards, Thermo Scientific).

Particle effective density was measured with an aerosol particle mass analyzer (APM, Kanomax) (Ehara et al. 1996) and a SMPS in series. The APM is located upstream of the SMPS for improved time resolution (~1 min) over the more common configuration of the differential mobility analyzer (DMA)—APM (McMurry et al. 2002; Khalizov et al. 2009; Xue et al. 2009). A detailed description of the APM–SMPS system and data algorithms are described elsewhere (Malloy et al. 2009). The 0.01–100 fg measurement range of the APM is equivalent to approximately 30–580 nm for particles with unit density (Kanomax Japan, Inc.). In this study, the APM setting was programmed to select 3–5 different particle masses (typically in 20 min) to obtain particle density as a function of particle mass. Fractal-like dimension was obtained by fitting the effective density versus size relationship into a power function (Park et al. 2003; Xue et al. 2009):

$$\rho_{eff} = C d_m^{D_f - 3} \quad [1]$$

TABLE 1
Engine load, initial concentrations, calculated OH concentration, $D_f$, bulk effective density, and overall dilution ratio

| Run | | Load | PM volume ($\mu m^3/cm^3$)[a] | PM number ($10^4$ $cm^{-3}$)[a] | Initial $NO_x$ (ppm)[a] | Initial ethene (ppb)[a] | Calculated OH (molec/$cm^3$)[b] | $D_f$ (Average $\pm$ $SD$)[c] | Bulk $\rho_{eff}$ ($g/cm^3$)[d] | Dilution ratio |
|---|---|---|---|---|---|---|---|---|---|---|
| Ejector dilution, short transfer line | | | | | | | | | | |
| 1 | 4/17/2010 | Idle | 68 | 3.9 | 0.76 | N.A. | N.A. | 2.52 → 2.81 | 0.70 | 114 |
| In-chamber dilution, short transfer line | | | | | | | | | | |
| 2 | 3/20/2010 | Idle | 195 | 9.3 | 1.60 | 150 | $1.4 \times 10^6$ | $2.97 \pm 0.05$ | 1.16 | 54 |
| 3 | 4/23/2010 | Idle | 22 | 2.5 | 0.24 | 32 | $1.6 \times 10^6$ | 2.65 → 2.83 | 0.84 | 362 |
| 4 | 5/7/2010 | Idle | 50 | 3.7 | 0.54 | 71 | $1.6 \times 10^6$ | 2.79 → 2.90 | 0.99 | 161 |
| Ejector dilution, long transfer line | | | | | | | | | | |
| 5 | 5/16/2009 | Medium | 94 | 2.4 | 0.57 | N.A. | N.A. | N.A. | N.A. | 409 |
| 6 | 11/13/2009 | Medium | 103 | 5.3 | 0.65 | N.A. | N.A. | $2.39 \pm 0.03$ | 0.49 | 359 |
| 7 | 11/16/2009 | Medium | 36 | 3.1 | 0.23 | N.A. | N.A. | $2.39 \pm 0.03$ | 0.49 | 1015 |
| 8 | 11/18/2009 | Medium | 53 | 3.7 | 0.30 | N.A. | N.A. | $2.35 \pm 0.05$ | 0.55 | 778 |
| 9 | 2/1/2010 | Low | 113 | 4.5 | 0.91 | 45 | $1.1 \times 10^6$ | $2.44 \pm 0.04$ | 0.51 | 176 |
| Ejector dilution, long transfer line, dark | | | | | | | | | | |
| 10 | 2/25/2010 | Idle | 94[e] | 5.2[e] | 0.30[d] | 76 | N.A. | 2.55 → 2.45 | 0.67 | 290 |
| 11 | 5/9/2009 | Medium | 124[e] | 4.9[e] | 0.92[d] | N.A. | N.A. | $2.38 \pm 0.03$ | 0.55 | 254 |
| 12 | 7/6/2010 | Medium | 74[e] | 5.0[e] | 0.45[d] | N.A. | N.A. | 2.40 → 2.20 | 0.62 | 519 |

Note: N.A., not acquired.
[a]Values when black lights were turned on.
[b]Calculated based on ethene decay.
[c]Calculated by power curve fit on effective density vs. mobility diameter (see text).
[d]Values when injection finished.
[e]Values 2 h after injection (typical time left in dark for aging experiments).



where $\rho_{eff}$ is the effective density of particles, $C$ is a constant, $d_m$ is the mobility diameter of particles, and $D_f$ is the fractal-like dimension.

Particle volatility was monitored with a volatility tandem DMA (VTDMA), in which monodisperse particles of mobility diameter $D_{mi}$ are selected by the 1st DMA followed by transport through a Dekati thermodenuder (TD, residence time: ~17 s, temperature: 100°C). The particle size after the TD ($D_{mf}$) is then measured by fitting a log-normal size distribution curve from the 2nd SMPS. Volume fraction remaining (VFR) is then calculated as the before and after the TD volume ratio, i.e., $VFR = (D_{mf}/D_{mi})^3$. Note that the "volume" in VFR measurement is based on mobility diameter measurement that includes void spaces in diesel agglomerates and caution must be taken in using VFR measurements to infer volatility of OA. The VTDMA was calibrated for each diameter setting using VFR of dry $(NH_4)_2SO_4$ seed aerosol and/or diesel particles at room temperature.

The chemical evolution of organic particulates was observed by a high-resolution time-of-flight aerosol mass spectrometer (HR-ToF-AMS) (Jayne et al. 2000; DeCarlo et al. 2006). The operation mode of the HR-ToF-AMS alternated between the mass spectrum (MS) W-mode and the particle time-of-flight (PToF) mode. Only the data from the MS mode is shown in this study. Recently developed elemental analysis (EA) software was used to track atomic ratio (O/C) of nonrefractory organic compounds (Aiken et al. 2008). Particle collection efficiency of the AMS is reported to be low for small (<70 nm) particles (Jayne et al. 2000). Although the geometric mean diameter (GMD) of the diesel exhaust particles was initially small (<70 nm), coagulation and/or preferential wall loss of these small particles caused the GMD to rapidly increase. The GMD during experiments was typically within 70–200 nm. The reported results of the AMS are relative to the organic and nitrate signals. The sulfate and ammonium signals were negligible (<1%).

Ethene concentration was measured by a gas chromatograph—flame ionization detector (GC-FID, Agilent Technology 6890) that is equipped with a PLOT column. $NO_x$, CO, and $O_3$ concentration was measured by Teledyne model 200E, 300E, and 400E analyzers, respectively.

## 3. RESULTS AND DISCUSSION

The engine load, initial concentrations (particle volume based on the SMPS measurement, $NO_x$, and ethene), calculated OH concentration (based on ethene decay rate), $D_f$, bulk effective density of particles, and dilution ratio are summarized in Table 1.

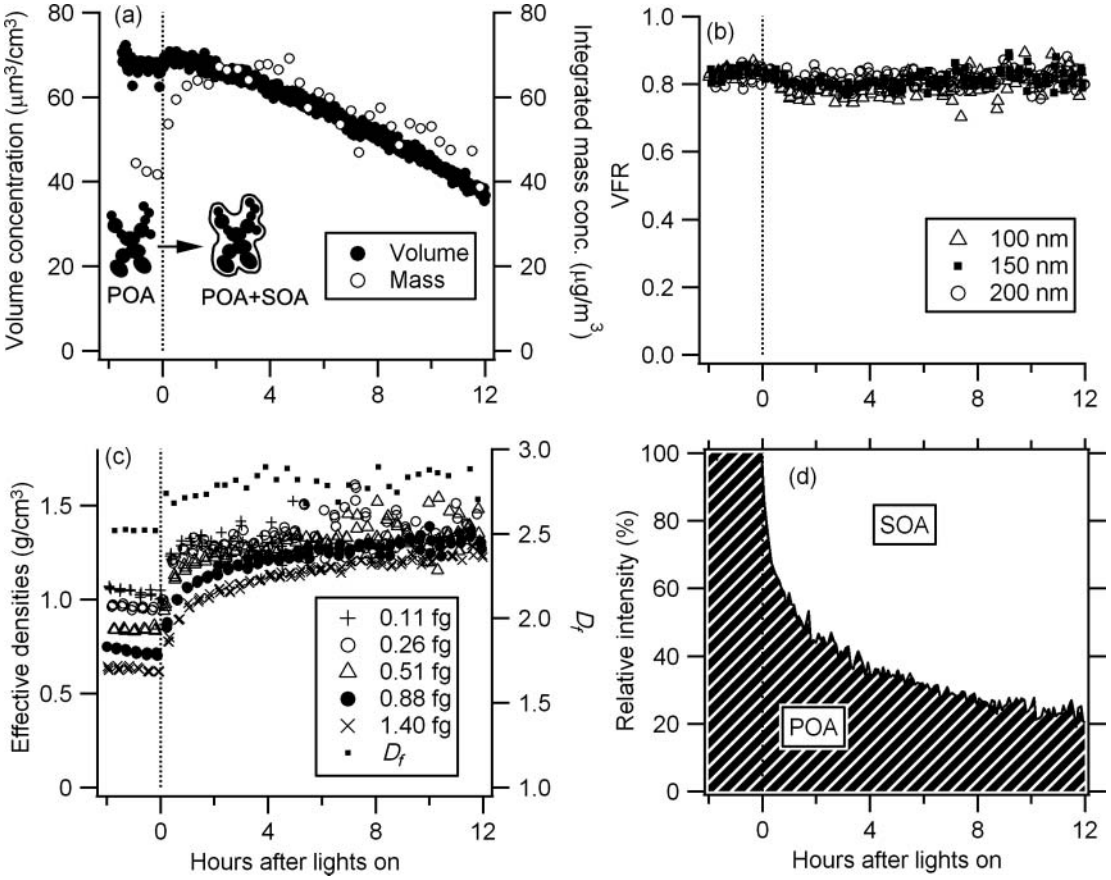


FIG. 2. Time series of (a) particle volume concentration and mass concentration, (b) volume fraction remaining (100°C), (c) effective density, fractal-like dimension ($D_f$), and (d) OA fraction. See text for detail (Results of Run 1) (conc.: concentration).



The dilution ratio is determined as the ratio of $NO_x$ concentration in the raw exhaust to that in the chamber.

Since the high NO concentration suppresses $O_3$ and $NO_3$ formation and ethene predominantly reacts with OH radical, exponential decay of ethene concentration was used to estimate OH radical concentration. The OH concentration was calculated to be 1–2 $\times$ $10^6$ molecule $cm^{-3}$, approximately equivalent to the 12-h daytime average ambient OH concentration level (Atkinson 2000). The OH concentration is in reasonable agreement with Weitkamp et al. (2007) (3 ($\pm$1) $\times$ $10^6$ molecule $cm^{-3}$).

Park et al. (2003) reported that particle fractal-like dimension somewhat increased as engine load decreased. Although the $D_f$ in Table 1 may indicate the same trend, it is difficult to draw any conclusion regarding the effect of load on $D_f$ due to the additional two parameters of the transfer line length and dilution method.

### 3.1. Interpretation of SOA Formation

Results of Run 1 (short transfer line, ejector dilution) are summarized in Figure 2. Only a minor increase of particle volume (wall loss uncorrected) was observed after the black lights were turned on, (Figure 2a). Also, the VTDMA measurement indicated little change in mobility diameter after passing through the TD that was set at 100°C (Figure 2b). However, particle effective densities increased rapidly (approximately 30%–80% within 2 h). The effective density and mobility diameter relationship was fit with a power function [Equation (1)] to determine $D_f$ (Figure 2c). The $D_f$ rapidly increased from 2.52 to 2.81 $\pm$ 0.06 after turning on the black lights. The fitted power function was used to interpolate/extrapolate particle density within the size range of the SMPS measurement. Particle mass concentration was calculated from particle volume and effective density as a function of mobility diameter. Calculated particle mass concentration is shown in Figure 2a.

The small increase in volume and small change in VFR, but significant increase in density and mass, during SOA formation are consistent with the filling of the void space of agglomerate particles by SOA. This is further confirmed by placing the TD in front of the APM–SMPS system (data not shown). Aging causes condensation of secondary organics; hence aged diesel particulates show a greater decrease in effective density after passing through the TD (compared with fresh particles) as they have more organic mass condensed onto their fractal agglomerate backbone. This demonstrates that particle volume measurement

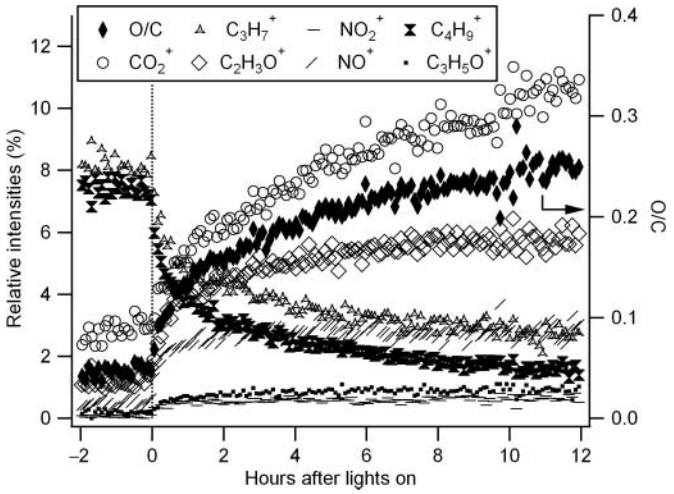


FIG. 3. Time series of selected ions measured by an AMS (Run 1).

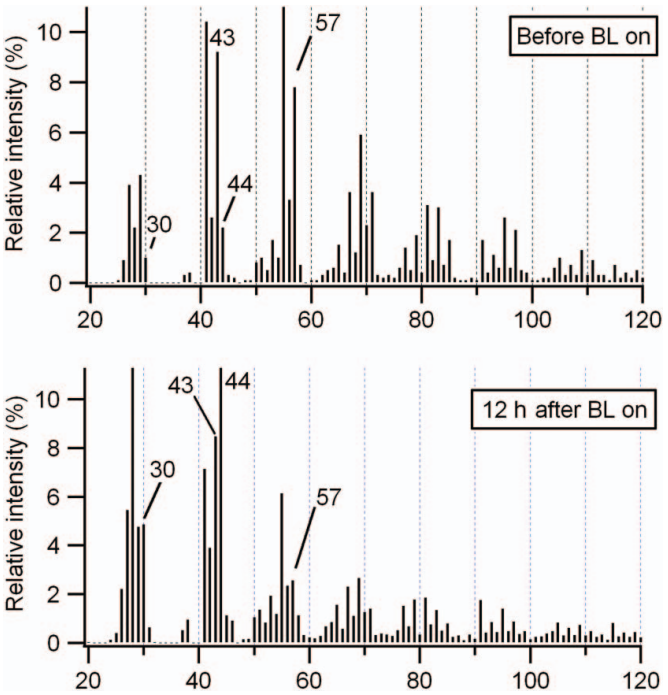


FIG. 4. Aerosol mass spectrums of diesel exhaust particulate before and after UV irradiation (Run 1) (BL: black light).

based only on mobility diameter can underestimate SOA formation from diesel exhaust.

The HR-ToF-AMS O/C measurement indicated that oxygenated species rapidly increased after black lights were turned on (Figure 3). Prior to photooxidation, the O/C ratio of the diesel exhaust particulate was 0.05. After the black lights were turned on, this ratio increased continuously to 0.25 within 12 h due to condensation of secondary organics onto the diesel agglomerate. The continuous increase of the O/C ratio is consistent with the continuous gas-phase oxidation of diesel exhaust reported by Sage et al. (2008) (based on the profile of m/z 44) and/or the cleavage of C–C bond (fragmentation) of large molecules (Kroll et al. 2009, 2011). MSs obtained by the HR-ToF-AMS before and after the UV irradiation are shown in Figure 4. Increase of m/z 44 (confirmed to be $CO_2^+$ fragment by high-resolution analysis) was observed. Also m/z 30 increased, which was largely ascribed to $NO^+$ fragment by high-resolution analysis, suggesting that the high $NO_x$ condition applied in this study led to formation of nitrogen containing species.

The AMS has also been used to estimate the contribution of SOA during other diesel exhaust studies (Weitkamp et al. 2007; Sage et al. 2008; Chirico et al. 2010). Sage et al. (2008) used m/z 57 (assumed to be $C_4H_9^+$) measured by the quadrupole-AMS (Q-AMS) as a tracer of POA. Chirico et al. (2010) pointed out that oxygen-containing species such as $C_3H_5O^+$ can also contribute to m/z 57. Therefore, they selected $C_4H_9^+$ by utilizing the high-resolution capability of the HR-ToF-AMS. In this study, $C_4H_9^+$ was also used as the tracer. As shown in Figure 3, $C_3H_5O^+$ significantly contributes to m/z 57 signal. However, the assumption of constant $C_4H_9^+$/POA ratio should be considered as a rough approximation since mass spectra of POA may change (Chirico et al. 2010). The fraction of SOA in organics was estimated by the following equation (Chirico et al. 2010):

$$\%\mathrm{SOA}(t) = [\mathrm{Org}(t) - (\mathrm{C_4H_9^+}(t)/\mathrm{C_4H_9^+}(t_0)) \times \mathrm{Org}(t_0)]/\mathrm{Org}(t) \quad [2]$$

The estimated SOA fraction is shown in Figure 2d. After 12 h of irradiation, 80% of OA was estimated to be SOA.

### 3.2. Effect of Injection Methods on Particle Physical Structure and Evolution

The previous section demonstrated that particle effective density measurement provides critical insight into the physical evolution of fractal particulate inside an environmental chamber. In this section, the impact of dilution method and transfer line length (Figure 1) on the measured physical and chemical evolution of diesel exhaust particulate is explored. The particle volume, mass concentration, and bulk effective density (mass concentration/volume concentration) for different injection/dilution conditions are shown in Figure 5.

The particle density was observed to be higher when raw exhaust was injected into the chamber (in-chamber dilution) than when dilute exhaust was injected (ejector dilution) (Figure 5c). The initial particle density was expected to be a function of the dilution ratio of the exhaust with more significant evaporation of semivolatile hydrocarbons occurring at a larger dilution ratio. However, the bulk effective density at varying dilution ratios (e.g., Runs 1–4, Figure 6) prove that dilution ratio by itself could not explain the low density in the

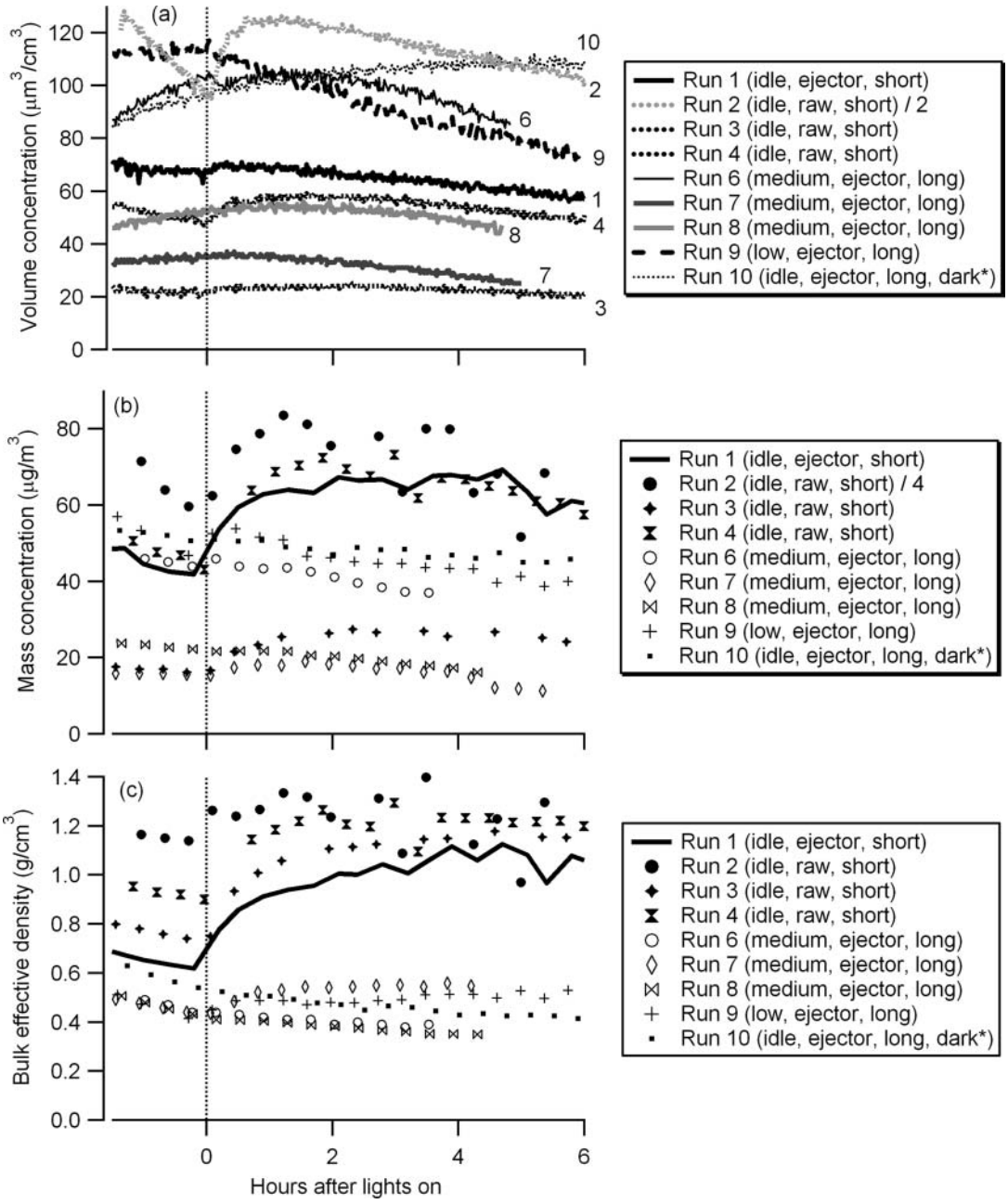


FIG. 5. Evolution of particle volume, mass concentration, and bulk effective density (*Lights were not turned on for Run 10 but shown for the sake of comparison. Time injection completed is set to −2 h.).

ejector-dilution experiment (Run 1). The density difference between in-chamber dilution and ejector-dilution experiments also could not be ascribed solely to the size dependence of density (Figure 2c) since the initial particle sizes did not systematically differ between dilution methods.

The differences in initial density values suggest that the relatively stagnant in-chamber dilution resulted in slower evaporation of semivolatiles compared with the ejector dilution. The ejector system creates rapid turbulent dilution of diesel exhaust with purified compressed air; this prediluted exhaust subsequently fills the empty chamber resulting in additional turbulence during the filling process. This may lead to faster evaporation of semivolatiles compared with the relatively stagnant method of injecting a puff of raw exhaust into chamber already filled with clean air. The previous work by Lipsky and Robinson (2005) showed an evaporation timescale of 2.5 s for diesel exhaust in a dilution sampler designed to induce turbulent mixing; Grieshop et al. (2009) showed that the evaporation timescale

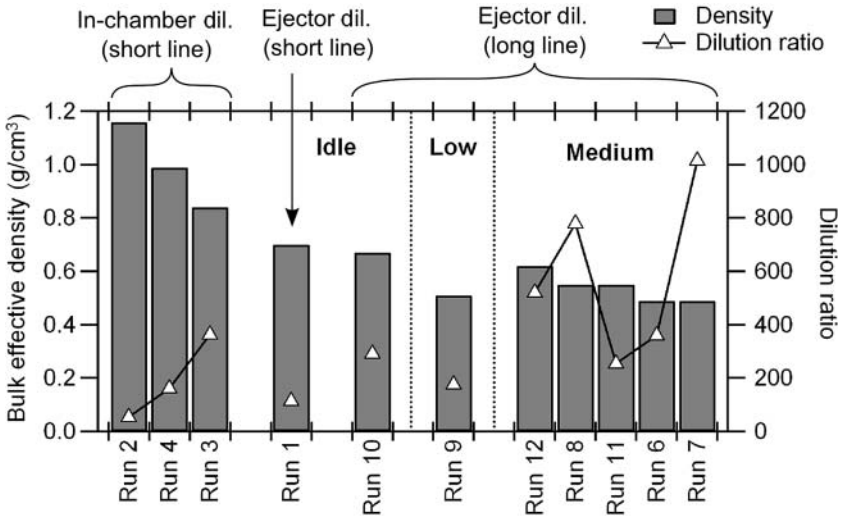


FIG. 6. Effective densities of particles in an environmental chamber and dilution ratio when the injection was completed (dil.: dilution).



of lubrication oil aerosols in a chamber was in the order of hours. This contrast suggests that evaporation of semivolatiles was kinetically inhibited, and hence, a more turbulent dilution method may enhance desorption of semivolatiles from fractal agglomerates. To our knowledge, this is the first time two different methods of dilution and filling of an environmental chamber have been compared and resulting effects on particle effective density investigated.

In Runs 5–12, exhaust was rapidly diluted and then transferred through a 16-m transfer line. The bulk effective densities for the medium load experiments were independent of the dilution ratio (Figure 6; Runs 6, 7, 8, 11, and 12). A similar trend was observed by Lipsky and Robinson (2006); for medium engine loads, elemental carbon (EC) dominated the carbon fraction, and hence, the impact of evaporation of semivolatile organics due to dilution on the particle mass was minor. Unlike Run 1 (Figure 2) and Runs 2–4, where exhaust was introduced through a shorter transfer line (∼2 m), the particle volume concentrations increased in the dark due to coagulation regardless of engine load. An example of particle volume evolution in the dark is shown in Figure 7. Since the particle mass concentration was confirmed to be decreasing due to wall loss (Figure 7), the increase of volume indicates particle coagulation leading to less dense particles. The volume increase is not likely due to condensation because the particles are highly fractal and condensing semivolatiles would have filled the void fraction of the fractal particle rather than lead to an increase in mobility diameter. Furthermore, after turning on the black lights, the particle volume did not respond to the SOA formation (Figure 5a), whereas the SOA formation was confirmed by the slight increase of particle mass concentration (Figure 5b). This is an obvious case where the particle volume measurement by the SMPS fails to represent SOA formation, and hence, mass-based measurement techniques are required. Since the mass evolution of Runs 1 and 10 (Figure 7) in the dark is similar, only mass-based analysis for those long transfer line experiments would provide insightful understanding towards SOA formation.

The increasing trend of particle volume in the dark is attributed to the fractal nature of the particles. As shown through the experiments in Figure 5 where the increasing volume in the dark was observed (Runs 6–12), the particle bulk effective densities were lower than in the other cases (Runs 1–4). Coagulation of fractal particles should lead to bigger, less dense particles. This is consistent with the concurrent

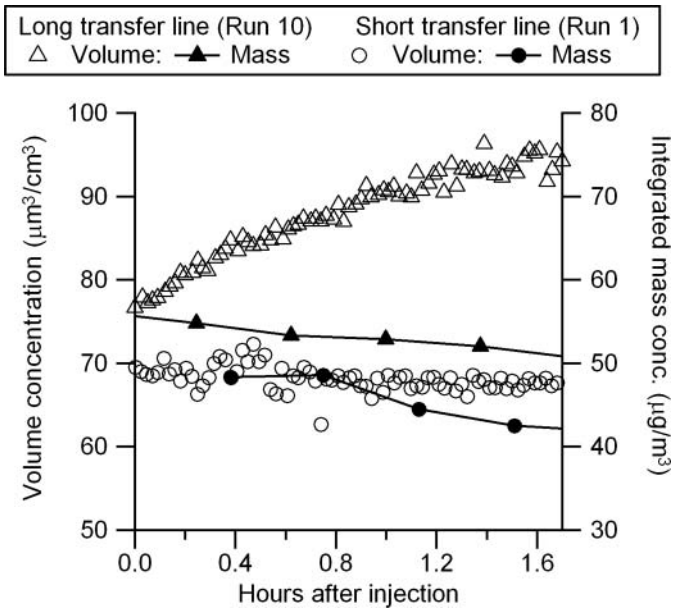


FIG. 7. Time series of particle volume and mass concentration before lights are turned on. Comparison of short transfer line (Run 1) and long transfer line (Run 10) experiments at idle (conc.: concentration).

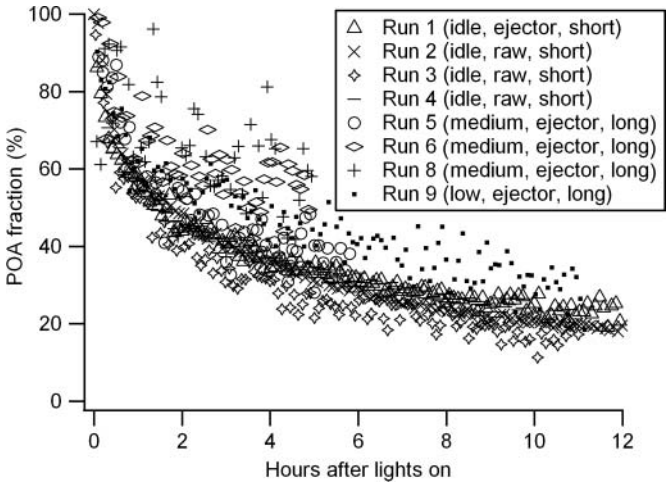


FIG. 8. Evolution of POA fraction calculated by the AMS $C_4H_9^+$ tracer method (Equation (2), see text).

observations of increasing particle volume concentration and decreasing mass concentration. Jacobson et al. (2005) noted that coagulation rates of fractal-like particles are faster than that of spherical particles. However, the fact that the density dissimilarity in Runs 1 and 10 was small but the dark volume evolution between the two cases was in the opposite direction (Figure 7) may suggest other unknown transfer line effects that enhance particle coagulation. The trend of continuously increasing volume along with decreasing bulk effective density in the dark was observed during all experiments using the long transfer line regardless of engine load (Runs 5–12).

The fraction of POA calculated by Equation (2) is compared for the experiments with different engine loads and injection methods (Figure 8). For all conditions, the POA fraction rapidly decreased due to SOA formation. The SOA fraction in Runs 6 and 8 were smaller than the other runs, which was consistent with the lower density measurement (Figure 5). While SOA formation was undetectable using the APM–SMPS for Runs 6 and 8, some SOA formation was detected in Run 7. This difference is attributed to experimental variability. The AMS MSs from Runs 6 to 8 (AMS not available for Run 7) were similar to the runs with higher SOA formation (major m/z including 30, 41, 43, 44, 55, and 57). Figure 8 indicates that approximately half of OA is composed of SOA during the first 2–5 h of photooxidation increasing to ∼80% within 12 h.

Particle (and possibly semivolatile) wall-loss correction was not performed in this study due to the uncertainties such as size-dependent wall-loss or coagulation of fractal particles. However, the POA/SOA split calculated by the AMS tracer method [Equation (2)] is independent of particle wall loss (Figure 8). The apparent abundance of SOA (∼80% within 12 h) highlights the importance of diesel exhaust as a source of SOA in an urban area. For the future, in addition to the series of measurement techniques employed in this study, an EC or black carbon (BC) measurement can help to constrain the carbon balance and particle wall loss (Chirico et al. 2010).

## 4. CONCLUSION

SOA was produced from dilute diesel exhaust following UV irradiation inside an environmental chamber. A unique setup of the APM–SMPS system enabled the determination of particle effective density as a function of particle mass, which in turn gave an improved insight into particle physical evolution during environmental chamber studies of diesel exhaust. The fractal-like dimension of diesel particulates was observed to be approximately 2.2–3.0 by the APM–SMPS, indicating the particle shape could either be fractal or nearly spherical depending on experimental conditions. Particle volume concentration was demonstrated to underestimate SOA formation due to the filling of void spaces of agglomerate particles. The HR-ToF-AMS measurement indicated O/C ratio increased rapidly right after turning on the black lights and continued to increase from 0.05 to 0.25 within 12 h. The AMS also showed that SOA contributed to 80% of OA mass within 12 h, emphasizing the importance of diesel exhaust as a source of urban SOA. When raw exhaust was injected into a nearly full chamber (in-chamber dilution), instead of injecting the diluted exhaust from an ejector diluter system into a nearly empty chamber (ejector dilution), the particle effective densities were observed to be higher; this was attributed to faster evaporation of semivolatile species by the intense mixing of an ejector diluter. For interpretation of SOA formation from diesel exhaust, it is critical to run a particle mass measurement since the volume measurement alone was found to be misleading in cases where particles are highly fractal.

## REFERENCES

Aiken, A. C., DeCarlo, P. F., Kroll, J. H., Worsnop, D. R., Huffman, J. A., Docherty, K., Ulbrich, I., Mohr, C., Kimmenl, J. R., Sun, Y., Zhang, Q., Trimborn, A. M., Northway, M., Ziemann, P. J., Canagaratna, M. R., Onasch, T. B., Alfarra, M. R., Prevot, A. S., Dommen, J., Duplissy, J., Metzger, A., Baltensperger, U., and Jimenez, J. L. (2008). O/C and OM/OC Ratios of Primary, Secondary, and Ambient Organic Aerosols with High-Resolution Time-of-Flight Aerosol Mass Spectrometry. *Environ. Sci. Technol.*, 42:4487–4485.

Atkinson, R. (2000). Atmospheric Chemistry of VOCs and $NO_x$. *Atmos. Environ.*, 34:2063–2101.

Chan, A. W. H., Kautzman, K. E., Chhabra, P. S., Surratt, J. D., Chan, M. N., Crounse, J. D., Kurten, A., Wennberg, P. O., Flagan, R. C., and Seinfeld, J. H. (2009). Secondary Organic Aerosol Formation from Photooxidation of Naphthalene and Alkylnaphthalenes: Implications for Oxidation of Intermediate Volatility Organic Compounds (IVOCs). *Atmos. Chem. Phys.*, 9:3049–3060.

Chirico, R., DeCarlo, P. F., Heringa, M. F., Tritscher, T., Richter, R., Prevot, A. S. H., Dommen, J., Weingartner, E., Wehrle, G., Gysel, M., Laborde, M., and Baltensperger, U. (2010). Impact of Aftertreatment Devices on Primary Emissions and Secondary Organic Aerosol Formation Potential from in-use Diesel Vehicles: Results from Smog Chamber Experiments. *Atmos. Chem. Phys.*, 10(23):11545–11563.

Cocker, D. R., Flagan, R. C., and Seinfeld, J. H. (2001). State-of the Art Chamber Facility for Studying Atmospheric Aerosol Chemistry. *Environ. Sci. Technol.*, 35(12):2594–2601.

Davidson, C. I., Phalen, R. F., and Solomon, S. (2005). Airborne Particulate Matter and Human Health: A Review. *Aerosol Sci. Technol.*, 39:737–749.

DeCarlo, P. F., Kimmel, J. R., Trimborn, A. M., Northway, M., Jayne, J. T., Aiken, A. C., Gonin, M., Fuhrer, K., Horvath, T., Docherty, K., Worsnop, D. R., and Jimenez, J. L. (2006). Field-Deployable, High-Resolution, Time-of-Flight Aerosol Mass Spectrometer. *Anal. Chem.*, 78:8281–8289.

Donahue, N. M., Robinson, A. L., and Pandis, S. N. (2009). Atmospheric Organic Particulate Matter: From Smoke to Secondary Organic Aerosol. *Atmos. Environ.*, 43:94–106.

Ehara, K., Hagwood, C., and Coakley, K. J. (1996). Novel Method to Classify Aerosol Particles According to Their Mass-to-Charge Ratio-Aerosol Particle Mass Analyzer. *J. Aerosol Sci.*, 27(2):217–234.

Eldering, A., and Cass, G. R. (1996). Source-Oriented Model for Air Pollutant Effects on Visibility. *J. Geophys. Res.*, 101(D14):19343–19369.

Grieshop, A. P., Miracolo, M. A., Donahue, N. M., and Robinson, A. L. (2009). Constraining the Volatility Distribution and Gas-Particle Partitioning of Combustion Aerosols Using Isothermal Dilution and Thermodenuder Measurements. *Environ. Sci. Technol.*, 43(13):4750–4756.

IPCC. (2007). *Intergovernmental Panel on Climate Change: Climate Change 2007: The Physical Science Basis*. Cambridge University Press, Cambridge, UK.

Jacobson, M. Z., Kittelson, D. B., and Watts, W. F. (2005). Enhanced Coagulation due to Evaporation and its Effect on Nanoparticle Evolution. *Environ. Sci. Technol.*, 39:9486–9492.

Jayne, J. T., Leard, D. C., Zhang, X., Davidovits, P., Smith, K. A., Kolb, C. E., and Worsnop, D. R. (2000). Development of an Aerosol Mass Spectrometer for Size and Composition Analysis of Sibmicron Particles. *Aerosol Sci. Technol.*, 33:49–70.

Kanakidou, M., Seinfeld, J. H., Pandis, S. N., Barnes, I., Dentener, F. J., Facchini, M. C., Van Dingenen, R., Ervens, B., Nenes, A., Nielsen, C. J., Swietlicki, E., Putaud, J. P., Balkanski, Y., and Wilson, J. (2005). Organic Aerosol and Global Climate Modelling: A Review. *Atmos. Chem. Phys.*, 5:1053–1123.

Khalek, I. A., Kittelson, D. B., and Brear, F. (2000). Nanoparticle Growth During Dilution and Cooling of Diesel Exhaust: Experimental Investigation and Theoretical Assessment. *SAE Technical Paper Series,* 2000-2001-0515.

Khalizov, A. F., Zhang, R., Zhang, D., Xue, H., Pagels, J., and McMurry, P. H. (2009). Formation of Highly Hygroscopic Soot Aerosols Upon Internal Mixing with Sulfuric Acid Vapor. *J. Geophys. Res.*, 114:D05208, doi: 10.1029/2008JD010595.

Kroll, J. H., Donahue, N. M., Jimenez, J. L., Kessler, S. H., Canagaratna, M., Wilson, K. R., Altieri, K. E., Mazzoleni, C., Wozniak, A. S., Bluhm, H., Mysak, E. R., Smith, J. D., Kolb, C. E., and Worsnop, D. R. (2011). Carbon Oxidation State as a Metric for Describing the Chemistry of Atmospheric Organic Aerosol. *Nature Chem.*, 3:133–139.

Kroll, J. H., Smith, D. F., Che, D. L., Kessler, S. H., Worsnop, D. R., and Wilson, K. R. (2009). Measurement of Fragmentation and Functionalization Pathways in the Heterogeneous Oxidation of Oxidized Organic Aerosol. *Phys. Chem. Chem. Phys.*, 11:8005–8014.

Lipsky, E. M., and Robinson, A. L. (2005). Design and Evaluation of a Portable Dilution Sampling System for Measuring Fine Particle Emissions from Combustion Systems. *Aerosol Sci. Technol.*, 39:542–553.

Lipsky, E. M., and Robinson, A. L. (2006). Effects of Dilution on Fine Particle Mass and Partitioning of Semivolatile Organics in Diesel Exhaust and Wood Smoke. *Environ. Sci. Technol.*, 40(1):155–162.

Malloy, Q., Nakao, S., Qi, L., Austin, R. L., Stothers, C., Hagino, H., and Cocker, D. R. (2009). Real-Time Aerosol Density Determination Utilizing a Modified Scanning Mobility Particle Sizer—Aerosol Particle Mass Analyzer system. *Aerosol Sci. Technol.*, 43:673–678.

Maricq, M. M., Podsiadlik, D. H., and Chase, R. E. (2000). Size Distributions of Motor Vehicle Exhaust PM: A Comparison Between ELPI and SMPS Measurements. *Aerosol Sci. Technol.*, 33:239–260.

McMurry, P. H., Wang, X. W., Park, K., and Ehara, K. (2002). The Relationship Between Mass and Mobility for Atmospheric Particles: A New Technique for Measuring Particle Density. *Aerosol Sci. Technol.*, 36:227–238.

Park, K., Kittelson, D. B., and McMurry, P. H. (2003). Relationship Between Particle Mass and Mobility for Diesel Exhaust Particles. *Environ. Sci. Technol.*, 37(3):577–583.

Pope, C. A., and Dockery, D. W. (2006). Health Effects of Fine Particulate Air Pollution: Lines that Connect. *J. Air Waste Manage. Assoc.*, 56:709–742.

Presto, A. A., Miracolo, M. A., Kroll, J. H., Worsnop, D. R., Robinson, A. L., and Donahue, N. M. (2009). Intermediate-Volatility Organic Compounds: A Potential Source of Ambient Oxidized Organic Aerosol. *Environ. Sci. Technol.*, 43:4744–4749.

Robinson, A. L., Donahue, N. M., Shrivastava, M. K., Weitkamp, E. A., Sage, A. M., Grishop, A. P., Lane, T. E., Pierce, J. R., and Pandis, S. N. (2007). Rethinking Organic Aerosols: Semivolatile Emissions and Photochemical Aging. *Science*, 315:1259–1262.

Sage, A. M., Weitkamp, E. A., Robinson, A. L., and Donahue, N. M. (2008). Evolving Mass Spectra of the Oxidized Component of Organic Aerosol: Results from Aerosol Mass Spectrometer Analyses of Aged Diesel Emissions. *Atmos. Chem. Phys.*, 8:1139–1152.

Samy, S., and Zielinska, B. (2010). Secondary Organic Aerosol Production from Modern Diesel Engine Emission. *Atmos. Chem. Phys.*, 10:609–625.

Schauer, J. J., Rogge, W. F., Hildemann, L. M., Mazurek, M. A., and Cass, G. R. (1996). Source Apportionment of Airbourne Particulate Matter Using Organic Compounds as Tracers. *Atmos. Environ.*, 30(22):3837–3855.

Shrivastava, M. K., Lipsky, E. M., Stanier, C. O., and Robinson, A. L. (2006). Modeling Semivolatile Organic Aerosol Mass Emissions from Combustion Systems. *Environ. Sci. Technol.*, 40(8):2671–2677.

Volkamer, R., Jimenez, J. L., Martini, F. S., Dzepina, K., Zhang, Q., Salcedo, D., Molina, L. T., Worsnop, D. R., and Molina, M. J. (2006). Secondary Organic Aerosol Formation from Anthropogenic Air Pollution: Rapid and Higher than Expected. *Geophys. Res. Lett.*, 33(L17811): doi: 10.1029/2006GL026899.

Weitkamp, E. A., Sage, A. M., Pierce, J. R., Donahue, N. M., and Robinson, A. L. (2007). Organic Aerosol Formation from Photochemical Oxidation of Diesel Exhaust in a Smog Chamber. *Environ. Sci. Technol.*, 41(20):6969–6975.

Xue, H., Khalizov, A. F., Wang, L., Zheng, J., and Zhang, R. (2009). Effects of Coating of Dicarboxylic Acids on the Mass-Mobility Relationship of Soot Particles. *Environ. Sci. Technol.*, 43:2787–2792.